

Fe(II)–Fe(III)-Bearing Phases As a Mineralogical Control on the Heterogeneity of Arsenic in Southeast Asian Groundwater

André Burnol, Laurent Charlet

▶ **To cite this version:**

André Burnol, Laurent Charlet. Fe(II)–Fe(III)-Bearing Phases As a Mineralogical Control on the Heterogeneity of Arsenic in Southeast Asian Groundwater. Environmental Science and Technology, 2010, 44 (19), pp.7541-7547. 10.1021/es100280h . hal-00521988

HAL Id: hal-00521988
https://brgm.hal.science/hal-00521988

Submitted on 7 Aug 2015

HAL is a multi-disciplinary open access archive for the deposit and dissemination of scientific research documents, whether they are published or not. The documents may come from teaching and research institutions in France or abroad, or from public or private research centers.

L'archive ouverte pluridisciplinaire **HAL**, est destinée au dépôt et à la diffusion de documents scientifiques de niveau recherche, publiés ou non, émanant des établissements d'enseignement et de recherche français ou étrangers, des laboratoires publics ou privés.

Fe(II)-Fe(III)-bearing Phases as a Mineralogical Control on the Heterogeneity of Arsenic in Southeast Asian Groundwater

ANDRE BURNOL [§‡*], *LAURENT CHARLET* [§]

§LGIT-OSUG, University of Grenoble-I, BP 53, F-38041 Grenoble Cedex 9, France.

‡ BRGM, Bureau de Recherches Géologiques et Minières, Environment and Process Division, 3, avenue Claude Guillemin, BP 36009, 45060 Orléans Cedex 2, France

In preparation for **Environmental Science & Technology**

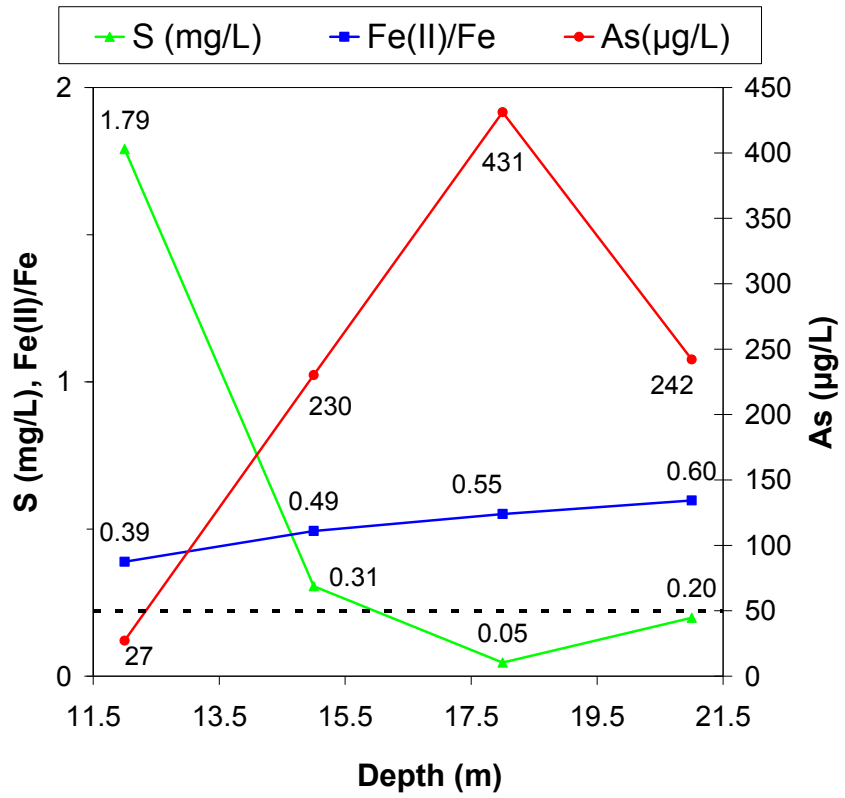
*Corresponding author

Phone: +33 238 644 647; fax: +33 238 643 062; e-mail address: a.burnol@brgm.fr

Abstract (word limit: 150-200 words) (192 words)

Although groundwater arsenic constitutes a major hazard to the health of the people of Southeast Asia, the exact mineralogical origin of the arsenic in these fluvial aquifers is still under debate. Fe(III) oxides are the dominant hosts of mobilizable arsenic in the sediments, with the role of secondary Fe(II)-bearing phases like mackinawite, siderite, vivianite, magnetite and carbonate green rust (fougerite) still unclear. Based on published field data from Chakdaha (India), the importance of the phases for arsenic mobility is evaluated quantitatively using models of growing complexity. Arsenic heterogeneity can be explained by the presence of two contrasted redox zones in the aquifers, with Fe(III) oxides being the dominant sorbent for arsenic in the less reduced zones and Fe(II) sulfides and/or Fe(II) carbonates being the solid-phase hosts for arsenic under more reduced conditions below impermeable soils or close to rivers where sulfate is reduced. A 1D reactive transport model which simulates the transition between the two environments has been developed and compared to field data. The results show that microbial sulfate reduction followed by abiotic and/or biotic reduction of As(III)-bearing iron oxides accounts for the spatial heterogeneity of arsenic in such reduced aquifers.

TOC Art


S (mg/L)
Fe(II)/Fe
As(µg/L)
S (mg/L), Fe(II)/Fe
As (µg/L)
Depth (m)
1.79
431
230
242
0.39
0.49
0.55
0.60
0.31
0.20
0.05
27
2
1
0
450
400
350
300
250
200
150
100
50
0
11.5
13.5
15.5
17.5
19.5
21.5

(less than 7000 words) (4480 words with references, 2 Tables, 4 Figures)

Introduction (2 double spaced pages with <20 references)

The spatial heterogeneity of arsenic in shallow groundwater is well documented in many fluvial regions of Southeast Asia and occurs on very small scales with high arsenic concentrations (>100 µg/L) commonly being found within tens of meters of low concentrations, i.e. below 50 µg/L, the drinking water standard in those areas. It reflects local heterogeneities in the water recharge, water chemistry and sediment properties inherent to a young depositional floodplain environment.

The most widely accepted mechanism causing high aqueous arsenic concentrations in Southeast Asian aquifers is the microbial reductive dissolution of iron (hydr)oxides and the concomitant release of arsenic *(1)*. The origin of the organic matter that drives such aquifers toward reducing conditions is, however, still under debate. Moreover, there is an observed decoupling of iron and arsenic release in both the laboratory *(2-4)* and the field *(1)*. This poor As-Fe correlation could be explained by various scenarios, such as (i) a biotic reduction of As(V) to As(III) which sorbs more weakly onto iron oxyhydroxides *(4)*, (ii) a precipitation of different secondary Fe(II) phases after the reductive dissolution of Fe(III) phases *(5)*, (iii) a weaker sorption of arsenic by the secondary Fe(II) phases (*(6)* and references therein).

The combination of local hydrology and geochemistry in those aquifers results in two contrasted geochemical environments: a moderately reduced environment characterized by low Fe(II)/Fe ratios with relatively high sulfate and low arsenic concentrations (<50 µg/L As), and a more reduced (hereafter termed "anoxic") environment characterized by higher Fe(II)/Fe ratios with lower sulfate and higher As concentrations. These two environments have been observed along the Mekong River in Cambodia *(7-9)*, along the Red River in Vietnam *(10)*, along a stream at the K site in Araihazar, Bangladesh *(11, 12)* and along the Hooghly River in Chakdaha, India *(13, 14)* (Figures 2SI and 3SI).

In these anoxic environments, arsenic mobility would be controlled by the nature and distribution of secondary Fe(II) or mixed Fe(II)/Fe(III) phases like mackinawite Fe(II)S, magnetite $Fe(II)Fe(III)_2O_4$, fougerite $Fe(II)_4Fe(III)_2(OH)_{12}CO_3.2H_2O$ (the mineral analogue of carbonate green rust), siderite $Fe(II)CO_3$ and vivianite $Fe(II)_3(PO_4)_2.8H_2O$ *(15-17)*.

The aim of the present paper is to infer from Chakdaha data (India) different scenarios of arsenic release using models of growing complexity like Kd sorption, surface complexation and 1D reactive transport models.

Models

Iron(III) surface complexation model. Geochemical speciation and sorption were performed with PHREEQC version 2.15 *(18)* using the WATEQ4F database *(19)*. The protonation constants of arsenite, being consistent with the sorption data calculated by Dixit and Hering *(20)*, were extracted from the MINEQL V4.5 database *(21)*. Only arsenite is considered because arsenate reduction is expected to precede crystallised iron (e.g. goethite, hematite) and sulphate reduction on a thermodynamic basis *(9)*. The interaction between arsenite and iron(III) surface is described by the two-layer surface complexation model from Dzombak and Morel *(22)* with only one type of adsorption site being considered, i.e. the weak sites ≡(w)FeOH (Table 1). Campbell et al. *(23)* estimated that the maximum surface site density for arsenic onto ferric hydroxides is [≡(w)FeOH] = 0.117 Fe_T with Fe_T the total solid Fe concentration. The amount of extractable iron in the sediments ranged from 1.6 to 9.7 wt.% at the Chakdaha site *(14)* but only a fraction of this iron is contained in mineral phases with available surface sites for arsenic. This available fraction, which includes amorphous phases (e.g. ferrihydrite) and also more crystalline Fe minerals (e.g. hematite, goethite), can be approximated by the reducible iron pool of the sediment, typically 10 to 20% of the solid phase iron, as opposed to the recalcitrant fraction (e.g. Fe incorporated in silicate minerals) *(24)*. The

reducible Fe fraction in our model is assumed to be 20 % of the total iron, i.e. 0.2 wt.% supposing 1 wt.% of iron in sediment.

1D generic reactive transport model. Coupling the geochemical reactions with a constant 1D advective flow was performed with PHREEQC version 2.15 *(18)* using the WATEQ4F database *(19)*. A high pore velocity of 5 cm/day (see SI), i.e. 5.8 10^{-7} m/s, is selected for simulating a generic 1D flow path from an area recharge to a depth range (e.g. the Wells I3-5-6-7).

The model's reaction processes at local equilibrium are aqueous speciation, surface complexation onto iron oxide (Table 1) and mineral dissolution/precipitation. Microbially mediated terminal electron accepting processes (TEAPs) are included in the model under kinetic constraints. A first order dependency for surface-complexed sulfide concentrations with respect to the abiotic reduction of iron could be considered (Table 2). The sorption of arsenic onto secondary phases (siderite or mackinawite) is included in the model using the Kd at pH 7 (Table 1) and a very high kinetics (Table 2, SI). The Michaelis-Menten and Monod kinetic approaches are traditionally used for modeling TEAPs coupled with transport *(25)*. A well-known shortcoming of this approach is that it does not account for the complete competitive exclusion or/and the thermodynamic feasibility of these TEAPs *(26, 27)*. In this generic study, the total rate of organic carbon oxidation (Rc) is determined independently from the concentration of species other than organic carbon. Rc is assumed to be representative of the average reactivity of the sedimentary organic carbon over the vertical range of interest and is broken down into the contributions of individual metabolic pathways represented by nitrate, sulfate and/or iron reduction (see SI). The sequential use of terminal electron acceptors based on differences in their redox potential can be simulated by defining critical concentrations of electron acceptors below which the model shifts to the next available electron acceptor. The limiting concentrations for NO_3^-, SO_4^{--}, Fe(III) and the initial concentrations are fitted values obtained by using data of Wells I3-5-6-7 (Tables 2 and 1SI).

The favorability of sulfate reduction could exceed the favorability of crystallized iron, e.g. goethite or hematite, at commonly observed Fe^{2+} concentrations in the Bengali aquifers *(9)*. In the scenario (a), it is supposed that nitrate, sulfate, and iron reduction are successive external electron acceptors, but without considering the abiotic reduction of Fe(III) by HS^-. Conversely, in scenario (b), the abiotic reduction of iron by HS^- is considered, but without considering dissimilatory iron reduction. Comparing the results of both scenarios will determine which respiration process could account for the release of arsenic.

Iron(II) Kd sorption model. Iron and arsenic total concentrations, respectively As_T and Fe_T, are assumed to be conserved between the two redox contrasted environments (see SI). The conservation between the two closed systems is described by the two following equations:

$$As_T = [As]_{\max} \times (1 + \sum_i M_i \times K_d^i) \quad (1)$$

$$Fe_T = \sum_i M_i \times f_i \quad (2)$$

where $[As]_{max}$ is a high aqueous concentration of As(III) in the anoxic environment (e.g. 5 µmol/L), M_i the mass of the i-th Fe(II)-bearing phase (mackinawite, vivianite, magnetite, fougerite, siderite), Kd^i the adsorption/partition coefficient for As(III) onto the i-th phase, and f_i the percentage of iron in the total weight of the i-th phase. Calculation of the Kd^i coefficients shows that, except for vivianite, Kd^i depends strongly on pH, in particular between pH 7 and 7.5 which is the variation range at the Chakdaha site *(28)*. The Kd^i coefficients are calculated from the adsorbed As fraction called s and the i-th solid concentration called d^i (g/L) obtained from the sorption isotherms published in the literature (see Tables 1 and 3SI):

$$K_d^i = \frac{s}{(1-s) \times d^i} \quad (3)$$

MATLAB® (R2006b, The MathWorks, Natick, MA) is used to solve the problem in cases with two, three or four sorbents. In every case, there are only two unknowns in eq 1 and in eq 2.

Results and Discussion

Field site. A transect of simultaneously collected groundwater and aquifer solids perpendicular to the banks of the Hooghly River in Chakdaha (West Bengal, India) was used to calibrate the different models (Figures 1 and 1SI). The methods of sample collection with the needle-sampler and chemical analysis are described by van Geen et al. *(29)* and a description of the analytical methods is given in SI.

Two contrasted redox environments in Chakdaha subsurface. Two contrasted redox environments are distinguished in Chakdaha subsurface *(13)*: fairly permeable sandy soils (indicated by low electromagnetic conductivity) where moderately reduced conditions prevail with low Fe(II)/Fe solid ratios (<0.5), underlain by more impermeable clayey soils (indicated by high electromagnetic conductivity) where more reduced conditions prevail with high Fe(II)/Fe solid ratios (>0.5). The sandy soils are also characterized by high permeability, a high concentration of sulfate ions (>1 mg/L S), and a low arsenic concentration (<50 μg/L As), whereas the underlying clayey soils are characterized by low permeability, a low sulfate concentration (<1 mg/L S), and a high arsenic concentration (>100 μg/L As). This contrast is particularly observed in I7 Well, with a negative correlation (-0.85) between aqueous arsenic and sulfate and a positive correlation (+0.9) between aqueous arsenic and solid Fe(II)/Fe ratio. The low Fe(II)/Fe ratio is attributed to iron-oxide coatings on quartz and mica sand particles, while the high Fe(II)/Fe solid ratio may be related to Fe(II)-rich minerals like Acid Volatile Sulfides (AVS; e.g. disordered mackinawite), as well as fine vivianite, siderite, fougerite and magnetite particles. These contrasted solid and aqueous environments play likely a role in the release of arsenic: the Fe(III) oxide vs. Fe(II) sulfide/carbonate solid phases correspond to high S(VI) vs. high As(III) aqueous phases.

In order to test different scenarios, geochemical computations were performed on two closed model systems; namely a Fe(III) oxide-As(III)-SO_4-water system known as the "Iron(III) surface complexation model" and a Fe(II) sulfide/carbonate-As(III)-H_2S-water system known as the "Iron(II) Kd sorption model". In the moderately reduced environment, solid iron is assumed to be the unique sorbent and arsenite the unique sorbate. In the anoxic environment, the Fe(II)-bearing phases (magnetite, siderite, fougerite, vivianite) are potential sorbents and As(III) the unique sorbate. A "1D generic reactive transport model" is developed to simulate the transition between these two environments.

Iron(III) surface complexation model. A typical low concentration of arsenic is set to 17 µg/L (Table 1SI) and the pH to 7, the mean pH at Chakdaha site *(14)*. The sorption equilibrium calculated by PHREEQC results in a total of 0.76 mmol sorbed As(III) L^{-1} as the sum of ≡(w)$FeHAsO_3^-$ and ≡(w)FeH_2AsO_3 (Table 2SI). Assuming a porosity of 0.25 and a density of 2.62, it corresponds to a sorbed arsenic concentration of 7.3 mg kg^{-1}. The sediment extraction by phosphates dislodges by anion exchange the relatively mobile fraction of As bound to Fe oxhydroxides and, potentially, As bound to adsorbed humic acids. This fraction within the Chakdaha sediments ranged from 0.5 to 9 mg kg^{-1} in Wells I3-5-6-7 (mean value 2.34 mg kg^{-1}) *(13)*. This surface model result is therefore consistent with the P-extractable arsenic data.

1D generic reactive transport model. The processes monitored in the above closed system are obviously not representative of those occurring in anoxic conditions: the release of arsenic depends not only on sorption interactions at local equilibrium but also on coupled reactive transport under kinetic constraints for redox sensitive elements like As, N, S, Fe. A reactive transport model was therefore developed in order to simulate a 1D flow path between the two contrasted redox systems. The calculation scheme results in smooth transitions between spatial redox zones as commonly observed *in situ (30)*. The oxidation rate of carbon C(0) is assumed to be constant along the 1D path

for nitrate and sulfate (see Model section). This oxidation rate is fixed to a maximum value of 2 mM $year^{-1}$ consistent with the observed range of 1.0-1.5 mM $year^{-1}$ for sulfate reduction found by Jakobsen et al. *(31)*. Assuming a constant carbon oxidation rate in scenario (a), the iron reduction rate would be 8 mM Fe $year^{-1}$ (one e^- consumed instead of 8 e^-). This "high" iron bioreduction rate is consistent with our previous batch experiments with amorphous 2-line ferrihydrite *(4)* but the iron reduction rate for crystallized iron, e.g. goethite, is very likely below the value for the amorphous phase like 2-line ferrihydrite *(32)*. A "low" rate of 1.5 mM Fe $year^{-1}$ was indeed fitted in scenario (a) using Well I7 (Figure 2).

The first result of (a) is that the maximum simulated concentration of As is in the range of the observed high arsenic concentrations (between 200 and 500 µg/L). A sensitivity analysis to pore velocity and to the Fe(III) reduction rate illustrates however that the maximum release of arsenic depends on the balance between the flow velocity and the chemical kinetics: a "low" flow velocity or a "high" Fe(III) reduction rate will both correspond to a dissolved arsenic peak slightly above 1 mg/L (Figure 4SI). Considering the uncertainty on both parameters at the Chakdaha site, the timescales the model fits are therefore probably not significant.

In scenario (a), the spatial profiles of the redox sensitive elements, i.e. the decrease of NO_3^-, SO_4^{--} and the increase of Fe(II) and As(III) along the 1D vertical path, are all correctly simulated (Figure 2) but the increase in alkalinity is slightly overestimated. The simulated Kd of arsenic onto siderite is closed to the Kd value at pH 7 (Table 1). The pore waters at the bottom of the profile in Wells I3-5-6-7 are undersaturated with respect to calcite and near from equilibrium with respect to siderite (except for I5). Combining all the samples during the period 2000-2002 showed however that the Chakdaha groundwaters are generally at local equilibrium with calcite and other carbonates (e.g. rhodochrosite, dolomite) and oversaturated with respect to siderite *(14)*.

In scenario (b), the aqueous As and solid Fe(2)/Fe are not consistent with the data (Figure 3). The comparison of both scenarios demonstrates that sulfate-reducing bacteria (SRB) activity alone is not sufficient and that iron-reducing bacteria (IRB) activity is needed to explain the release of arsenic in these Wells. The comparison shows also that the simulated chemical zones are quite different: (a) shows a transition between the sulfidic and ferruginous zones; in (b), HS- reduces solid Fe(III) and thus does not accumulate despite active sulfate reduction, whilst producing Fe(II) precipitates as siderite in the sulfate reduction zone. Sulfides were not measured during this campaign but there was no significant smelling during the sampling and a sulfidic zone is therefore unlikely. Moreover, a sediment vertical profile in Cambodia revealed siderite in a deep reduced zone that is not preceded by a sulfidic zone *(9)*. Finally, it shows that a more appropriate scenario could be the combining of both scenarios (see SI and Figure 5SI).

In the last scenario, termed (c), a concurrent dissimilatory reduction of iron and sulfate as already observed in field studies *(30)* or at micro-scale *(33)* is tested (see SI). In that case, the precipitation of FeS(s) removes HS^- and Fe^{2+} and therefore increases the favorability of both reducers (IRB and SRB) by increasing the energy gain. The arsenic aqueous profile in (c) is consistent with the data (Figure 3). Therefore, a concurrent bacterial respiration process between IRB and SRB can not be excluded.

Alternative biogeochemical mechanisms omitted in 1D model. Other (bio)geochemical processes may consume carbonates and are not considered in this simplified model like the methanogenesis or/and the rhodochrosite precipitation *(14)*. Moreover, our approach clearly shortcuts the multiple steps of the complex organic matter breakdown: the kinetic rate of carbon oxidation is assumed to be constant. The past decade has seen a large number of models that couple the kinetic expressions with the thermodynamic constraints, either in the fermentation step or in the terminal electron accepting reaction step. One of the most used representations is the so-called “partial redox disequilibrium” model, first developed by McNab and Narasimhan *(34)*. The idea is to separate

organic matter degradation into only two steps. The first step comprises hydrolyzation and fermentation, producing labile organic carbon, nutrients and inorganic carbon HCO_3^-; the produced number of inorganic moles per mole of labile organic carbon is generally unknown. The key point is that this first step limits the overall rate and that the second step is the terminal electron reactions step, which is faster and close to equilibrium.

Iron(II) Kd sorption model in Southeast Asian aquifers: a sensitivity analysis. The concentration of solid As ranges between 2 and 22 mg kg^{-1} *(14)*. A typical sediment with about 1 wt.% of Fe-oxides and about 2 mg kg^{-1} of solid As is considered (see SI). The one-phase systems (with a unique sorbent for arsenite) and the multiple-phase systems (with different sorbents) have been systematically investigated (Table 4SI).

In the one-phase systems, an abundance of around 15 wt.% Fe in mackinawite is needed. This result is much higher than the observed values of AVS in Araihazar (Bangladesh), where AVS varies from 0.2 to 2 µmol g^{-1} sediment (J. Métral, personal communication); AVS represents only 0.11 to 1.1 wt.% iron assuming about 1 wt.% iron in the sediment.

Using Kd at pH 7 and 7.5, a similar calculation shows that between 56 wt.% and 84 wt.% iron in siderite is needed, assuming that siderite is the dominant host for arsenite. This result is a little higher than observed ratios of between 35% and 40% found in Cambodian sediments *(9)*. The groundwater in the shallow reducing aquifers is strongly supersaturated for both vivianite $Fe(II)_3(PO_4)_2.8H_2O$ and hydroxyapatite $Ca_5(PO_4)_3OH$ in Bangladesh *(24)* and also supersaturated for vivianite in Vietnam *(35)*. The highest concentration of P derived from sandy horizons of the Bengal basin was reported to be equal to 214 mg P/kg *(36)*. Assuming that vivianite is the dominant Fe-bearing host of sedimentary phosphorus, then vivianite represents only around 6 wt.% Fe (see SI). Conversely, if we assume that vivianite is the unique sorbent for arsenite, then 87 wt.% of iron in vivianite is needed. The conclusion is that vivianite, mackinawite and magnetite are likely not the dominant host for arsenite at

pH 7 and that siderite is the better candidate as the main sorbent (at least in the short list investigated in this work).

In multiple-phase systems, the residual iron is assumed to be distributed within two, three or four Fe(II)-bearing phases: if mackinawite represents 1 wt.% of the solid iron and if furthermore the dominant hosts of arsenite are siderite and magnetite, then an abundance of 74 wt.% siderite and 25 wt.% magnetite are needed at pH 7 (see SI). Two possible four-phase systems are shown in Figure 4 with a similar calculated Fe(II)/Fe ratio (0.83 with magnetite or 0.9 with fougerite). The main conclusion for one-phase systems is still valid with multiple-phase systems: siderite seems to be the better candidate as the dominant host for arsenite at pH 7.

Implication for arsenic heterogeneity in reducing aquifers. We first demonstrate that low concentrations of arsenic in moderately reduced zones at the Chakdaha site could be explained by a adsorption of As(III) onto solid Fe(III) oxides. We then hypothesize that the observed high concentrations of arsenic in the anoxic zones could be quantitatively interpreted by a reduction of solid Fe(III) oxides followed by sorption of As(III) on different Fe(II)-bearing phases: while Fe(II) sulfide (e.g. disordered mackinawite) or vivianite are not the dominant host for arsenite, the ferrous carbonates (like siderite or/and fougerite) very likely play a major role in such reduced systems. We finally simulate the transition between the two contrasted redox zones and compare different energetically possible scenarios of arsenic release. This comparison shows that the reduction of solid iron by biogenic sulfides is not sufficient to explain this release. The reactive transport model shows also that both scenarios, assuming a successive or a concomitant sulfate and iron reduction, are consistent with the observations at Chakdaha site.

Acknowledgments

The authors gratefully acknowledge RGNDWM, Govt. of India, IFCPAR and CNRS (EC2CO Programme) for giving financial support. One of the authors (AB) is thankful to the Bureau de Recherches Géologiques et Minières (BRGM) for supporting this publication work and to Nolwenn Croiset for helpful discussions about Phreeqc modeling.

Supporting Information Available

This information is available free of charge via the internet at http://pubs.acs.org/.

References

1. Nickson, R.T.; McArthur, J.M.; Ravenscroft, P.; Burgess, W.G.; Ahmed, K.M. Mechanism of arsenic release to groundwater, Bangladesh and West Bengal. *Appl. Geochem.* **2000,** *15,* 403-413.

2. Islam, F.S.; Gault, A.G.; Boothman, C.; Polya, D.A.; Charnock, J.M.; Chatterjee, D.; Lloyd, J.R. Role of metal-reducing bacteria in arsenic release from Bengal delta sediments. *Nature* **2004,** *430,* 68-71.

3. van Geen, A.; Rose, J.; Thoral, S.; Garnier, J.M.; Zheng, Y.; Bottero, J.Y. Decoupling of As and Fe release to Bangladesh groundwater under reducing conditions. Part II: Evidence from sediment incubations. *Geochim. Cosmochim. Acta* **2004,** *68,* 3475-3486.

4. Burnol, A.; Garrido, F.; Baranger, P.; Joulian, C.; Dictor, M.; Bodenan, F.; Morin, G.; Charlet, L. Decoupling of arsenic and iron release from ferrihydrite suspension under reducing conditions: a biogeochemical model. *Geochemical Transactions* **2007,** *8,* 12.

5. Horneman, A.; van Geen, A.; Kent, D.V.; Mathe, P.E.; Zheng, Y.; Dhar, R.K.; O'Connell, S.; Hoque, M.A.; Aziz, Z.; Shamsudduha, M. Decoupling of As and Fe release to Bangladesh groundwater under reducing conditions. Part I: Evidence from sediment profiles. *Geochim. Cosmochim. Acta* **2004,** *68,* 3459-3473.

6. Charlet, L. and Polya, D.A. Arsenic in shallow, reducing groundwaters in southern Asia: an environmental health disaster. *Elements* **2006,** *2,* 91-96.

7. Polizzotto, M.L.; Kocar, B.D.; Benner, S.G.; Sampson, M.; Fendorf, S. Near-surface wetland sediments as a source of arsenic release to ground water in Asia. *Nature* **2008,** *454,* 505-508.

8. Kocar, B.D.; Polizzotto, M.L.; Benner, S.G.; Ying, S.C.; Ung, M.; Ouch, K.; Samreth, S.; Suy, B.; Phan, K.; Sampson, M.; Fendorf, S. Integrated biogeochemical and hydrologic processes driving arsenic release from shallow sediments to groundwaters of the Mekong delta. *Appl. Geochem.* **2008,** *23,* 3059-3071.

9. Kocar, B.D. and Fendorf, S. Thermodynamic Constraints on Reductive Reactions Influencing the Biogeochemistry of Arsenic in Soils and Sediments. *Environ. Sci. Technol.* **2009,** *43,* 4871-4877.

10. Eiche, E.; Neumann, T.; Berg, M.; Weinman, B.; van Geen, A.; Norra, S.; Berner, Z.; Trang, P.T.K.; Viet, P.H.; Stüben, D. Geochemical processes underlying a sharp contrast in groundwater arsenic concentrations in a village on the Red River delta, Vietnam. *Appl. Geochem.* **2008,** *23,* 3143-3154.

11. van Geen, A.; Zheng, Y.; Goodbred, S.; Horneman, A.; Aziz, Z.; Cheng, Z.; Stute, M.; Mailloux, B.; Weinman, B.; Hoque, M.A.; Seddique, A.A.; Hossain, M.S.; Chowdhury, S.H.; Ahmed, K.M. Flushing History as a Hydrogeological Control on the Regional Distribution of Arsenic in Shallow Groundwater of the Bengal Basin. *Environ. Sci. Technol.* **2008,** *42,* 2283-2288.

12. Radloff, K.A.; Manning, A.R.; Mailloux, B.; Zheng, Y.; Moshiur Rahman, M.; Rezaul Huq, M.; Ahmed, K.M.; Geen, A.v. Considerations for conducting incubations to study the mechanisms of As release in reducing groundwater aquifers. *Appl. Geochem.* **2008,** *23,* 3224-3235.

13. Metral, J.; Charlet, L.; Bureau, S.; Mallik, S.; Chakraborty, S.; Ahmed, K.; Rahman, M.; Cheng, Z.; van Geen, A. Comparison of dissolved and particulate arsenic distributions in shallow aquifers of Chakdaha, India, and Araihazar, Bangladesh. *Geochemical Transactions* **2008,** *9,* 1.

14. Nath, B.; Chakraborty, S.; Burnol, A.; Stüben, D.; Chatterjee, D.; Charlet, L. Mobility of arsenic in the sub-surface environment: An integrated hydrogeochemical study and sorption model of the sandy aquifer materials. *Journal of Hydrology* **2009,** *364,* 236-248.

15. Thinnappan, V.; Merrifield, C.M.; Islam, F.S.; Polya, D.A.; Wincott, P.; Wogelius, R.A. A combined experimental study of vivianite and As (V) reactivity in the pH range 2–11. *Appl. Geochem.* **2008,** *23,* 3187-3204.

16. Jönsson, J. and Sherman, D.M. Sorption of As(III) and As(V) to siderite, green rust (fougerite) and magnetite: Implications for arsenic release in anoxic groundwaters. *Chemical Geology* **2008,** *255,* 173-181.

17. Wolthers, M.; Charlet, L.; van Der Weijden, C.H.; van der Linde, P.R.; Rickard, D. Arsenic mobility in the ambient sulfidic environment: Sorption of arsenic(V) and arsenic(III) onto disordered mackinawite. *Geochim. Cosmochim. Acta* **2005,** *69,* 3483-3492.

18. Parkhurst, D.L.; Appelo, C.A.J. *User's guide to Phreeqc (version 2)- a computer program for speciation, batch-reaction, one-dimensional transport, and inverse geochemical calculation;* USGS: Denver, 1999.

19. Ball, J.W.; Nordstrom, D.K. *User's Manual for WATEQ4F, with Revised Thermodynamic Data Base and Test Cases for Calculating Speciation of Major, Trace, and Redox Elements in Natural Waters;* USGS: Denver, 1991.

20. Dixit, S. and Hering, J.G. Comparison of arsenic(V) and arsenic(III) sorption onto iron oxide minerals: Implications for arsenic mobility. *Environ. Sci. Technol.* **2003,** *37,* 4182-4189.

21. Schecher, W.D.; McAvoy, D.C. *MINEQL+, V4.5, Users Manual;* Hallowell: ME, 1998.

22. Dzombak, D.A.; Morel, F.M.M. *Surface Complexation Modeling: Hydrous Ferric Oxide;* John Wiley & Sons: New York, 1990.

23. Campbell, K.M.; Malasarn, D.; Saltikov, C.W.; Newman, D.K.; Hering, J.G. Simultaneous Microbial Reduction of Iron(III) and Arsenic(V) in Suspensions of Hydrous Ferric Oxide. *Environ. Sci. Technol.* **2006,** *40,* 5950-5955.

24. Swartz, C.H.; Blute, N.K.; Badruzzman, B.; Ali, A.; Brabander, D.; Jay, J.; Besancon, J.; Islam, S.; Hemond, H.F.; Harvey, C.F. Mobility of arsenic in a Bangladesh aquifer: Inferences from geochemical profiles, leaching data, and mineralogical characterization. *Geochim. Cosmochim. Acta* **2004,** *68,* 4539-4557.

25. Hunter, K.S.; Wang, Y.; Van Cappellen, P. Kinetic modeling of microbially-driven redox chemistry of subsurface environments: coupling transport, microbial metabolism and geochemistry. *J. Hydrol. (Amst.)* **1998,** *209,* 53-80.

26. Curtis, G.P. Comparison of approaches for simulating reactive solute transport involving organic degradation reactions by multiple electron acceptors. *Computers & Geosciences* **2003,** *29,* 319-329.

27. Heimann, A.; Jakobsen, R.; Blodau, C. Energetic Constraints on H2-Dependent Terminal Electron Accepting Processes in Anoxic Environments: A Review of Observations and Model Approaches. *Environ. Sci. Technol.* **2010,** *44,* 24-33.

28. Charlet, L.; Chakraborty, S.; Appelo, C.A.J.; Roman-Ross, G.; Nath, B.; Ansari, A.A.; Lanson, M.; Chatterjee, D.; Mallik, S.B. Chemodynamics of an arsenic "hotspot" in a West Bengal aquifer: A field and reactive transport modeling study. *Appl. Geochem.* **2007,** *22,* 1273-1292.

29. van Geen, A.; Protus, T.; Cheng, Z.; Horneman, A.; Seddique, A.A.; Hoque, M.A.; Ahmed, K.M. Testing Groundwater for Arsenic in Bangladesh before Installing a Well. *Environ. Sci. Technol.* **2004,** *38,* 6783-6789.

30. Postma, D. and Jakobsen, R. Redox zonation; equilibrium constraints on the Fe(III)/SO_4 - reduction interface. *Geochim. Cosmochim. Acta* **1996,** *60,* 3169-3175.

31. Jakobsen, R. and Cold, L. Geochemistry at the sulfate reduction–methanogenesis transition zone in an anoxic aquifer—A partial equilibrium interpretation using 2D reactive transport modeling. *Geochim. Cosmochim. Acta* **2007,** *71,* 1949-1966.

32. Bonneville, S.; Van Cappellen, P.; Behrends, T. Microbial reduction of iron(III) oxyhydroxides: effects of mineral solubility and availability. *Chem. Geol.* **2004,** *212,* 255-268.

33. Motelica-Heino, M.; Naylor, C.; Zhang, H.; Davison, W. Simultaneous Release of Metals and Sulfide in Lacustrine Sediment. *Environ. Sci. Technol.* **2003,** *37,* 4374-4381.

34. McNab, W.W., J. and Narasimhan, T.N. Modeling reactive transport of organic compounds in groundwater using a partial redox disequilibrium approach. *Water Resour. Res. 30,* 2619-2635.

35. Postma, D.; Larsen, F.; Minh Hue, N.T.; Duc, M.T.; Viet, P.H.; Nhan, P.Q.; Jessen, S. Arsenic in groundwater of the Red River floodplain, Vietnam: Controlling geochemical processes and reactive transport modeling. *Geochim. Cosmochim. Acta* **2007,** *71,* 5054-5071.

36. BGS; DPHE *Arsenic contamination of groundwater in Bangladesh;* D. G. Kinniburgh, P. L. Smedley, Eds; BGS: Keyworth, 2001.

37. Afonso, M.D. and Stumm, W. Reductive Dissolution of Iron(III) (Hydr)oxides by Hydrogen-Sulfide. *Langmuir* **1992,** *8,* 1671-1675.

38. Poulton, S.W. Sulfide oxidation and iron dissolution kinetics during the reaction of dissolved sulfide with ferrihydrite. *Chem. Geol.* **2003,** *202,* 79-94.

39. Wolthers, M.; Charlet, L.; van Der Linde, P.R.; Rickard, D.; van Der Weijden, C.H. Surface chemistry of disordered mackinawite (FeS). *Geochim. Cosmochim. Acta* **2005,** *69,* 3469-3481.

40. Bruno, J.; Wersin, P.; Stumm, W. On the influence of carbonate in mineral dissolution: II. The solubility of FeCO3 (s) at 25°C and 1 atm total pressure. *Geochim. Cosmochim. Acta* **1992,** *56,* 1149-1155.

41. Al-Borno, A. and Tomson, M. The temperature dependence of the solubility product constant of vivianite. *Geochimica et Cosmochimica Acta* **1994,** *58,* 5373-5378.

Table 1. Reactions used in "Iron(III) surface complexation model" and "Iron(II) Kd sorption model'

"Iron(III) surface complexation model"	**log K (I=0 M, 25 °C)**	**Reference**
$H_3AsO_3^{\circ} = H_2AsO_3^- + H^+$	-9.22	*(21)*
$H_2AsO_3^- = HAsO_3^{2-} + H^+$	-12.11	*(21)*
$HAsO_3^{2-} = AsO_3^{3-} + H^+$	-13.41	*(21)*
$\equiv(w)FeOH + H^+ = \equiv(w)FeOH_2^+$	7.29	*(22)*
$\equiv(w)FeOH = \equiv(w)FeO^- + H^+$	-8.93	*(22)*
$\equiv(w)FeOH + AsO_3^{3-} + 3H^+ = \equiv(w)FeH_2AsO_3 + H_2O$	38.76	*(20)*
$\equiv(w)FeOH + AsO_3^{3-} + 2H^+ = \equiv(w)FeHAsO_3^- + H_2O$	31.87	*(20)*
$\equiv(w)FeOH + HS^- = \equiv(w)FeS^- + H_2O$	5.3	*(37)*
$\equiv(w)FeOH + HS^- + H^+ = \equiv(w)FeHS + H_2O$	10.82	*(37)*
"Iron(II) Kd sorption model"	**Kd in L/g at pH 7 (7.5)**	**Reference**
H_3AsO_3 sorption on mackinawite	2 (2)	*(17)*
H_3AsO_3 sorption on siderite	0.267 (0.4)	*(16)*
H_3AsO_3 sorption on magnetite	0.081 (0.215)	*(16)*
H_3AsO_3 sorption on fougerite	0.095 (0.57)	*(16)*
H_3AsO_3 sorption on vivianite	0.18 (0.18) [a]	*(15)*

[a] experimental Kd for As(V) is assumed valid for As(III)

Table 2. Biogeochemical reactions included in the "1D generic reactive transport model"

Terminal electron accepting processes (biotic pathways)	**$[EA]_{lim}$ [b]**	**Maximum reduction rate (C(0) oxidation rate [a]) mM/year**	**Reference**
Denitrification $4/5NO_3^- + 1/2C_2H_3O_2^- + 3/10H^+ \rightarrow 2/5N_2 + HCO_3^- + 1/5H_2O$	14 mg/L [b]	8/5 (2 [a])	see text
Sulfate reduction $1/2SO_4^{2-} + 1/2C_2H_3O_2^- + 1/2H^+ \rightarrow 1/2H_2S + HCO_3^-$	0.5 mg/L [b]	1 (2 [a])	*(31)*
Iron reduction $4FeOOH + 1/2C_2H_3O_2^- + 15/2H^+ \rightarrow HCO_3^- + 4Fe^{2+} + 6H_2O$	42 mM [b]	"High rate" 8 (2 [a]) "Low rate" 1.5 (0.375 [a])	see text
Secondary redox reaction (abiotic pathway)		**Kinetic rate mn^{-1}**	
$HS^- + 5H^+ + 2FeOOH \rightarrow S° + 2Fe^{2+} + 4H_2O$		k=1/40	*(38)*, see SI
Precipitation reactions (non redox)	**logK**		
Mackinawite + $H^+ = Fe^{2+} + HS^-$	-2.95		*(39)*
Siderite + $H^+ = Fe^{2+} + HCO_3^-$	-0.47		*(40)*
Vivianite = $3Fe^{2+} + 2PO_4^{3-} + 8H_2O$	-35.77		*(41)*
Calcite + $H^+ = Ca^{2+} + HCO_3^-$	1.85		*(19)*
Adsorption reactions		**Kinetic rate s^{-1}**	
H_3AsO_3 sorption on mackinawite and siderite	-	k=1/100	see Table 1

[a] C(0) oxidation rate is assumed to be constant along the 1D path for nitrate, sulfate and iron reduction and fixed to 2 mM/year corresponding to 1 mM/year for sulfate reduction (see SI). The "high value" 8 mM/year for iron reduction is tested in the sensitivity analysis (see SI) while the "low value" 1.5 mM/year is the fitted value used in scenario (a)

[b] All the concentration limits for Electron Acceptors $[EA]_{lim}$ are fitted values

FIGURE CAPTIONS

FIGURE 1. Google Earth satellite image [http://earth.google.com/] of the study area (Chakdaha) in West Bengal, India. Symbols indicate the positions of needle-sampler profiles I1-I7 along the Hooghly River transect. Because of the oxidation-reduction (redox) conditions, the data material of this study is restricted to the Wells I7, I6, I5, I3 indicated by the red symbols (see SI).

FIGURE 2. Comparison of the results of the simulated scenario (a) with the porewater profiles of As, Fe, S, HCO_3^- and NO_3^- from the Well I7 (open square), Well I6 (open delta), Well I5 (open circle), Well I3 (open diamond). S is calculated from the SO_4^{2-} determinations by ion chromatography *(13)*. In order to compare all the Wells data with the 1D model, a reference depth Z0 is chosen for each Well (see Table 1SI). The solid lines represent aqueous predictions at the time where aqueous As reached its maximum value in scenario (a) with the "low" iron reduction rate (see Table 2 and main text). The simulated Saturation Indices (SI) of calcite and siderite are deduced from the alkalinities measured by titration. The dotted line is the simulated Kd of As onto siderite.

FIGURE 3. Comparison of the depth distribution of chemical zones and respiration processes in three scenarios (see text for details): in scenario (a), nitrate reduction precedes successive dissimilatory sulfate and Fe reduction; in scenario (b), nitrate reduction precedes sulfate reduction and abiotic Fe reduction by HS^-; in scenario (c), nitrate reduction precedes concomitant dissimilatory Fe and sulfate reduction (see SI). In scenario (a), the dissimilatory Fe(III) reduction rate is fixed to the "low value" of 1.5 mM/year. In the left-hand graphs, S(-II), Fe(II) and As(III) are represented at the time when aqueous As(III) reached its maximum value in each scenario, by the dashed-dotted, dashed and solid lines, respectively. In the right-hand graphs, solid Fe(III), mackinawite, siderite concentrations and Fe(II)/Fe molar ratio are shown at this time with the dotted, dashed-dotted, dashed and solid lines, respectively. The aqueous As and Fe(II)/Fe ratios of Wells I3, I5, I6, I7 are also shown with open square, delta, circle and diamond, respectively. In all scenarios, vivianite is not allowed to precipitate.

FIGURE 4. Two possible four-phase systems calculated in "Iron(II) Kd sorption model" at pH 7: mackinawite represents 1 wt.% Fe, vivianite 6 wt.% Fe (see SI) and the other possible phases are siderite and magnetite (or fougerite).

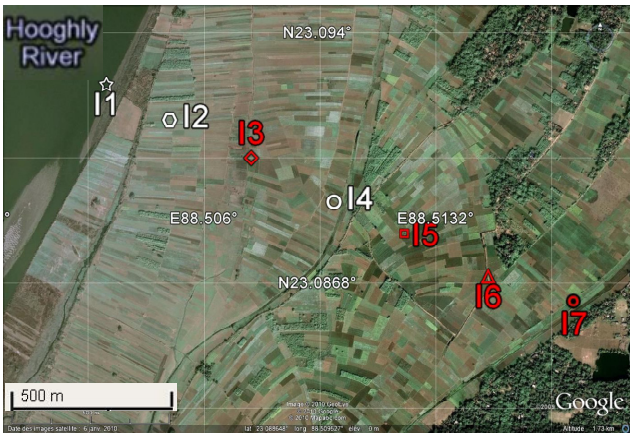

Hooghly River
N23.094°
I1
I2
I3
I4
E88.506°
E88.5132°
I5
N23.0868°
I6
I7
500 m
Google

FIGURE 1

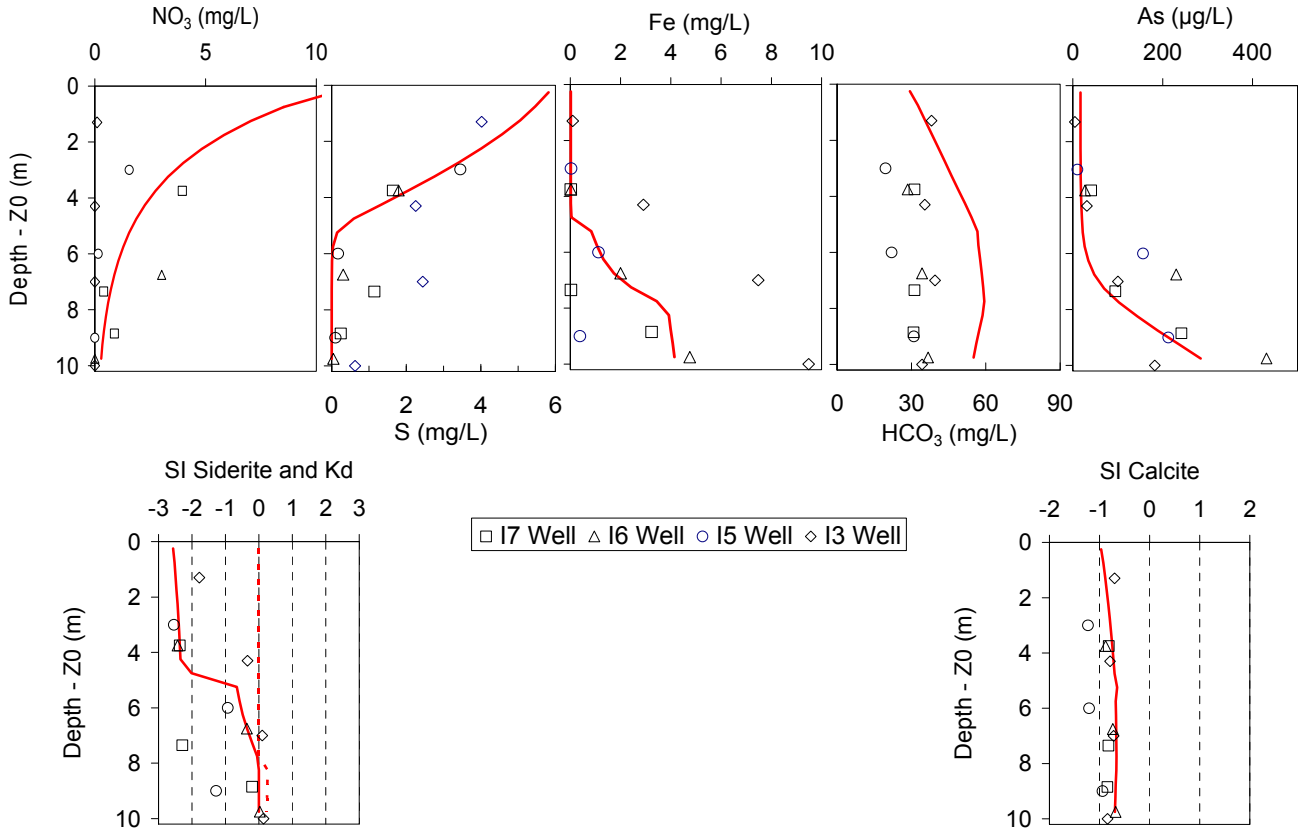

NO3 (mg/L)
Fe (mg/L)
As (µg/L)
Depth - Z0 (m)
S (mg/L)
HCO3 (mg/L)
SI Siderite and Kd
SI Calcite
I7 Well
I6 Well
I5 Well
I3 Well

FIGURE 2

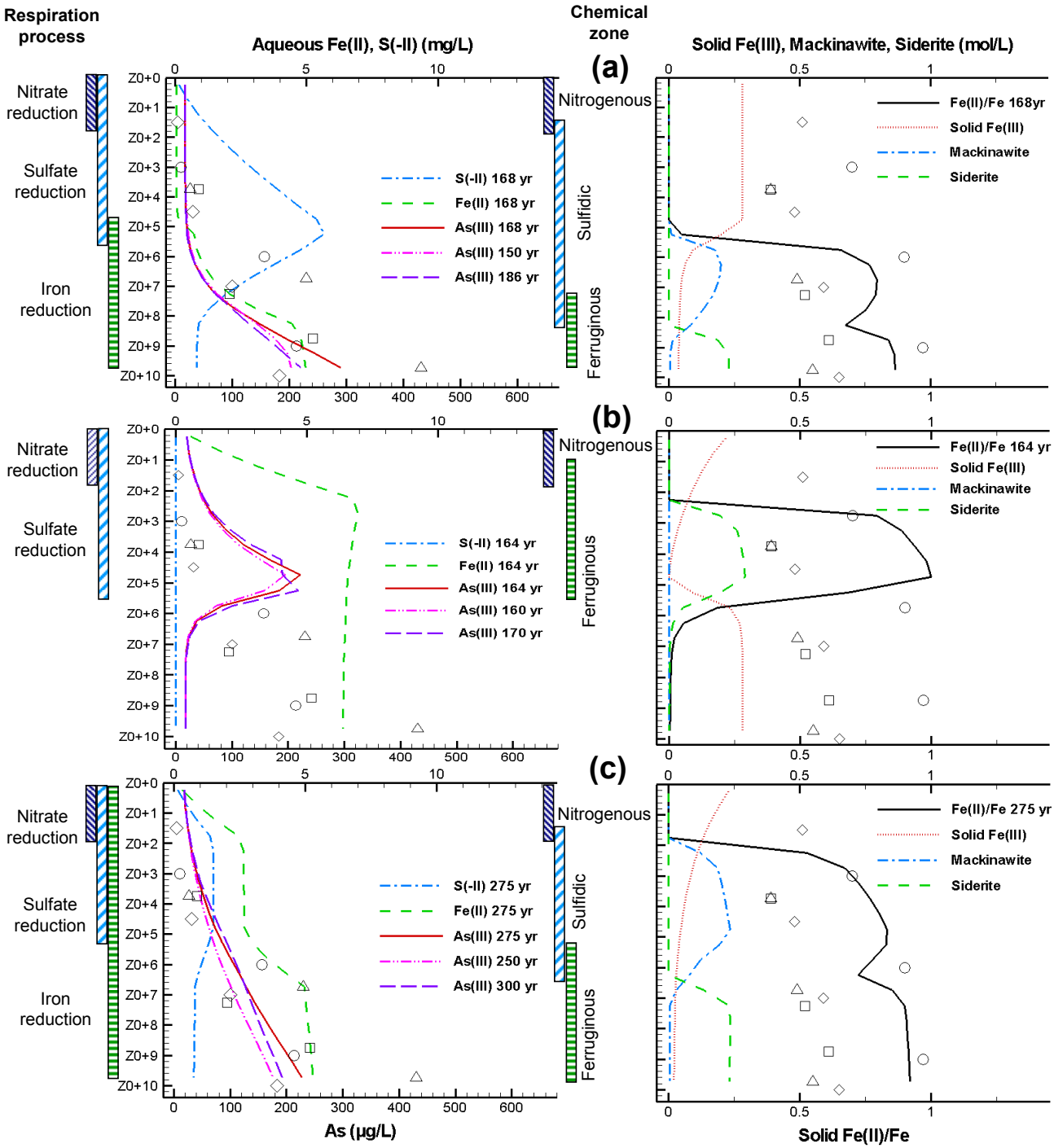

Respiration process
Chemical zone
Aqueous Fe(II), S(-II) (mg/L)
Solid Fe(III), Mackinawite, Siderite (mol/L)
(a)
(b)
(c)
Nitrate reduction
Sulfate reduction
Iron reduction
Nitrogenous
Sulfidic
Ferruginous
S(-II) 168 yr
Fe(II) 168 yr
As(III) 168 yr
As(III) 150 yr
As(III) 186 yr
Fe(II)/Fe 168yr
Solid Fe(III)
Mackinawite
Siderite
S(-II) 164 yr
Fe(II) 164 yr
As(III) 164 yr
As(III) 160 yr
As(III) 170 yr
Fe(II)/Fe 164 yr
S(-II) 275 yr
Fe(II) 275 yr
As(III) 275 yr
As(III) 250 yr
As(III) 300 yr
Fe(II)/Fe 275 yr
As (µg/L)
Solid Fe(II)/Fe

FIGURE 3

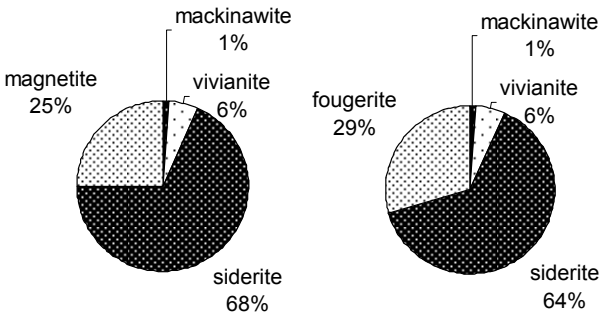

mackinawite
1%
magnetite
25%
vivianite
6%
siderite
68%
mackinawite
1%
fougerite
29%
vivianite
6%
siderite
64%

FIGURE 4

Brief: The nature and distribution of iron-bearing minerals has a prominent impact on arsenic mobilization in Southeast Asian groundwater